



OPEN

Storage and retrieval of $(3 + 1)$ -dimensional weak-light bullets and vortices in a coherent atomic gas

SUBJECT AREAS:
NONLINEAR OPTICS
SOLITONSZhiming Chen¹, Zhengyang Bai¹, Hui-jun Li^{2,1}, Chao Hang¹ & Guoxiang Huang¹Received
19 September 2014Accepted
8 December 2014Published
3 February 2015Correspondence and
requests for materials
should be addressed to
G.H. (gxhuang@phy.
ecnu.edu.cn)¹State Key Laboratory of Precision Spectroscopy and Department of Physics, East China Normal University, Shanghai 200062, China, ²Institute of Nonlinear Physics and Department of Physics, Zhejiang Normal University, Jinhua 321004, Zhejiang, China.

A robust light storage and retrieval (LSR) in high dimensions is highly desirable for light and quantum information processing. However, most schemes on LSR realized up to now encounter problems due to not only dissipation, but also dispersion and diffraction, which make LSR with a very low fidelity. Here we propose a scheme to achieve a robust storage and retrieval of weak nonlinear high-dimensional light pulses in a coherent atomic gas via electromagnetically induced transparency. We show that it is available to produce stable $(3 + 1)$ -dimensional light bullets and vortices, which have very attractive physical property and are suitable to obtain a robust LSR in high dimensions.

The investigation of light storage and retrieval (LSR), a key technique for realizing optical quantum memory, has received much attention in recent years^{1–3}. One of important techniques for LSR is electromagnetically induced transparency (EIT)⁴, a quantum interference effect typical occurring in a three-level atomic system interacting with a probe and a control laser fields. The origination of EIT is the existence of dark state, which makes not only the absorption (dissipation) of the probe field largely suppressed but also the LSR possible through an adiabatical manipulation of the control field.

Up to now, nearly all studies on LSR have been carried out in various schemes working in linear regime^{5,6}. Such schemes are simple but encounter the inevitable problem of pulse spreading due to the existence of dispersion, which may result in a serious distortion for retrieved pulse. Recently, the EIT-based LSR has been generalized to weak nonlinear regime, where the storage and retrieval of a $(1 + 1)$ -dimensional $[(1 + 1)D]$ (i.e., the first ‘1’ refers to one spatial dimension, and the second ‘1’ refers to time) soliton pulse is suggested^{7,8}. However, because the $(1 + 1)D$ soliton pulse is unstable in high dimensions due to the existence of diffraction, such scheme is still not realistic or quite limited. For practical applications of optical quantum memory, a challenged problem is to obtain a light pulse that is robust (i.e., with a high fidelity) during storage and retrieval in $(3 + 1)D$.

Before proceeding, we note that in recent years there is much effort focused on high-dimensional optical solitons due to their rich nonlinear physics and important applications^{9,10}. Although in recent works^{11–13} $(3 + 1)D$ light bullets and vortices in coherent atomic systems have been studied, the possibility of their storage and retrieval is not explored yet to the best of our knowledge.

Here we propose an EIT-based new scheme to realize a robust LSR for $(3 + 1)D$ light pulses in a coherent atomic ensemble working in a free space. Based on Maxwell-Bloch equations governing the evolution of atoms and light field we derive a nonlinear equation controlling the motion of the envelope of a probe field. We show the possibility for obtaining $(3 + 1)D$ light bullets (or called $(3 + 1)D$ spatiotemporal optical solitons^{9,10}) and vortices, which have ultraslow propagating velocity and extremely low generation power. We further show that these high-dimensional light pulses can be stabilized by using the balance between dispersion, diffraction, nonlinearity, and by a far-detuned laser field. We demonstrate that these high-dimensional light pulses can be stored and retrieved very stably by switching off and on a control field.

Results

Model. We consider a cold, lifetime-broadened Λ -type three-level atomic gas interacting with a probe field (with pulse length τ_0 , center angular frequency ω_p , and half Rabi frequency Ω_p) that drives the $|1\rangle \leftrightarrow |3\rangle$ transition, and a continuous-wave control field (with the center angular frequency ω_c and half Rabi frequency Ω_c) that drives $|2\rangle \leftrightarrow |3\rangle$ transition; see the inset of Fig. 1(a).

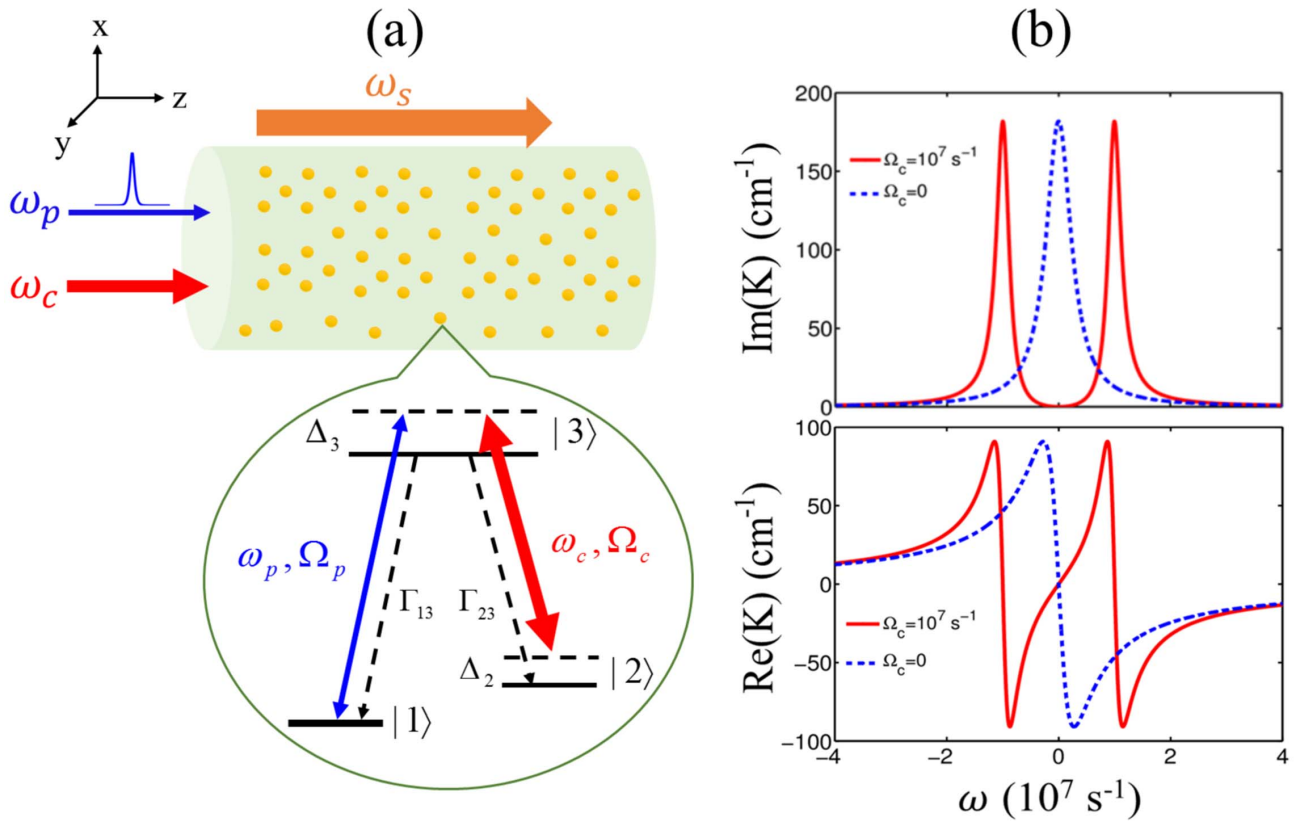


Figure 1 | Model and linear dispersion relation. (a) Possible experimental arrangement of beam geometry. The probe (with angular frequency ω_p and half Rabi frequency Ω_p) and continuous-wave control (with angular frequency ω_c and half Rabi frequency Ω_c) fields propagate nearly along z direction. The (orange) thick arrow denotes the Stark field (with angular frequency ω_s) used to stabilize (3 + 1)D light bullets and vortices. Cold atomic gas are represented by yellow dots. The inset shows the energy-level diagram and excitation scheme of the Λ -type three-level atoms. Δ_2 and Δ_3 are detunings, Γ_{13} (Γ_{23}) is the decay rate from $|3\rangle$ to $|1\rangle$ ($|3\rangle$ to $|2\rangle$). The atoms are initially populated on the ground state $|1\rangle$. (b) The linear dispersion relation $K(\omega)$ of the probe field as a function of ω .

For simplicity, we assume the electric field propagates along z direction with the form $\mathbf{E} = \sum_{l=p,c} \mathbf{e}_l \mathcal{E}_l e^{i(k_l z - \omega_l t)} + \text{c.c.}$, where \mathbf{e}_l (\mathcal{E}_l) is the unit polarization vector (envelope). A far-detuned laser field (Stark field) used to stabilize (3 + 1)D light bullets and vortices (see below) is applied to the system [see Fig. 1(a)] with the form $\mathbf{E}_{\text{Stark}}(x, y, t) = \mathbf{e}_s \sqrt{2} E_s(x, y) \cos(\omega_s t)$, where \mathbf{e}_s , E_s , and ω_s are the unit polarization vector, field amplitude, and angular frequency, respectively. Due to the existence of the Stark field, an energy shift for the level $|j\rangle$ occurs, i.e., $\Delta E_{j,\text{Stark}} = -\alpha_j \langle \mathbf{E}_{\text{Stark}}^2 \rangle_t / 2 = -\alpha_j |E_s(x, y)|^2 / 2$. Here α_j is the scalar polarizability of the level $|j\rangle$, and $\langle \dots \rangle$ denotes the time average in one oscillating cycle.

Under electric-dipole and rotating-wave approximations, the Hamiltonian of the system in the interaction picture reads $\hat{\mathcal{H}}_{\text{int}} = -\sum_{j=1}^3 \hbar \Delta'_j |j\rangle \langle j| - \hbar [\Omega_p |3\rangle \langle 1| + \Omega_c |3\rangle \langle 2| + \text{H.c.}]$, with $\Delta'_j = \Delta_j + [\alpha_j / (2\hbar)] |E_s|^2$, $\Omega_p = (\mathbf{e}_p \cdot \mathbf{p}_{13}) \mathcal{E}_p / \hbar$, and $\Omega_c = (\mathbf{e}_c \cdot \mathbf{p}_{23}) \mathcal{E}_c / \hbar$. Here $\Delta_2 = \omega_p - \omega_c - \omega_{21}$ and $\Delta_3 = \omega_p - \omega_{31}$ are respectively the two- and one-photon detunings, \mathbf{p}_{jl} is the electric-dipole matrix element related to the levels $|j\rangle$ and $|l\rangle$, $\hbar \omega_{jl} = E_j - E_l$ is the energy difference between the level $|j\rangle$ and the level $|l\rangle$ with E_j the eigen-energy of the level $|j\rangle$.

The equation of motion for density matrix σ in the interaction picture reads

$$\left(\frac{\partial}{\partial t} + \Gamma \right) \sigma = -\frac{i}{\hbar} [\hat{\mathcal{H}}_{\text{int}}, \sigma], \quad (1)$$

where σ is a 3×3 density matrix, Γ is a 3×3 relaxation matrix denoting the spontaneous emission and dephasing. The explicit expressions of Eq. (1) are presented in Methods.

The equation of motion for Ω_p can be obtained by the Maxwell equation $\nabla^2 \mathbf{E} - (1/c^2) \partial^2 \mathbf{E} / \partial t^2 = [1/(\epsilon_0 c^2)] \partial^2 \mathbf{P} / \partial t^2$, where $\mathbf{P} = \mathcal{N}_a \{ \mathbf{p}_{13} \sigma_{31} \exp[i(k_p z - \omega_p t)] + \mathbf{p}_{23} \sigma_{32} \exp[i(k_c z - \omega_c t)] + \text{c.c.} \}$ with \mathcal{N}_a the atomic concentration. Under slowly varying envelope approximation, the Maxwell equation is reduced to ref. 14

$$i \left(\frac{\partial}{\partial z} + \frac{1}{c} \frac{\partial}{\partial t} \right) \Omega_p + \frac{c}{2\omega_p} \left(\frac{\partial^2}{\partial x^2} + \frac{\partial^2}{\partial y^2} \right) \Omega_p + \kappa_{13} \sigma_{31} = 0, \quad (2)$$

where $\kappa_{13} = \mathcal{N}_a \omega_p |\mathbf{p}_{13} \cdot \mathbf{e}_p|^2 / (2\epsilon_0 c \hbar)$, with c the light speed in vacuum.

Our model can be realized by selecting realistic physical systems. One of them is the ultracold ^{87}Rb atomic gas with the energy levels selected as $|1\rangle = |5^2S_{1/2}, F=1\rangle$, $|2\rangle = |5^2S_{1/2}, F=2\rangle$, and $|3\rangle = |5^2P_{1/2}, F=2\rangle$, respectively. The decay rates are given by $\Gamma_2 \simeq 2\pi \times 1.0$ kHz, and $\Gamma_3 \simeq 2\pi \times 5.75$ MHz, and $\mathbf{p}_{13} \simeq \mathbf{p}_{23} = 2.54 \times 10^{-27}$ C cm¹⁵. If atomic density $\mathcal{N}_a = 1.1 \times 10^{11}$ cm⁻³, κ_{13} takes the value of 3.0×10^9 cm⁻¹ s⁻¹.

Nonlinear envelope equation. We use the standard method of multiple scales developed for EIT system¹⁴ to derive the nonlinear envelope equation for the probe field based on the asymptotic expansion of the Maxwell-Bloch (MB) Eqs. (1) and (2) (see Methods).



The first-order solution of the asymptotic expansion reads $\Omega_p^{(1)} = Fe^{i\theta}$, $\sigma_{j1}^{(1)} = \{[\delta_{j3}(\omega + \Delta_2 + i\gamma_{21}) - \delta_{j2}\Omega_c^*]/D\}Fe^{i\theta}$. Here $D = |\Omega_c|^2 - (\omega + \Delta_2 + i\gamma_{21})(\omega + \Delta_3 + i\gamma_{31})$ and $\theta = K(\omega)z_0 - \omega t_0$, with $K(\omega) = \omega/c + \kappa_{13}(\omega + \Delta_2 + i\gamma_{21})/D$ (linear dispersion relation). Note that the frequency and wave number of the probe field are respectively given by $\omega_p + \omega$ and $k_p + K(\omega)$, so $\omega = 0$ corresponds to the center frequency of probe field.

Fig. 1(b) shows the imaginary and real parts of $K(\omega)$, i.e., $\text{Im}(K)$ and $\text{Re}(K)$. The dashed and solid lines are for $\Omega_c = 0$ and for $\Omega_c = 1.0 \times 10^7 \text{ s}^{-1}$, respectively. From the upper panel we see that for $\Omega_c = 0$ (with no EIT) the probe pulse suffers a large absorption (the dashed line), whereas for $\Omega_c = 1.0 \times 10^7 \text{ s}^{-1}$ (with EIT) a transparency window opens and hence the probe pulse is nearly free of absorption (the solid line). The lower panel of Fig. 1(b) shows the drastic change of dispersion due to EIT, which results in a significant reduction of the group velocity of the probe pulse.

The solvability condition at the second order of the asymptotic expansion is $i[\partial F/\partial z_1 + (\partial K/\partial \omega)\partial F/\partial t_1] = 0$, which means that the probe-pulse envelope F travels with the group velocity $V_g = (\partial K/\partial \omega)^{-1}$. The nonlinear envelope equation for F is obtained from the solvability condition at the third order, i.e.,

$$i \frac{\partial F}{\partial z_2} - \frac{1}{2} \frac{\partial^2 K}{\partial \omega^2} \frac{\partial^2 F}{\partial t_1^2} + \frac{c}{2\omega_p} \left(\frac{\partial^2}{\partial x_1^2} + \frac{\partial^2}{\partial y_1^2} \right) F + W_{11}|F|^2 Fe^{-2az_2} + W_{12}|E_s^{(1)}|^2 F = 0, \quad (3)$$

where W_{11} is the self-phase modulation coefficient of the probe field and W_{12} is the cross-phase modulation coefficient contributed by the Stark field. The explicit expressions of W_{11} and W_{12} are given in Methods.

Combining the solvability conditions (i.e., the equations for F) at the all orders, we obtain the unified equation for F , which can be written into the dimensionless form

$$i \frac{\partial u}{\partial s} + \frac{1}{2} \left(g_1 \frac{\partial^2}{\partial \tau^2} + \frac{\partial^2}{\partial \xi^2} + \frac{\partial^2}{\partial \eta^2} \right) u + g_2 |u|^2 u + g_3 V(\xi, \eta) u = 0, \quad (4)$$

with $u = \epsilon F/U_0$, $s = z/L_{\text{Diff}}$, $\tau = [t - z/\text{Re}(V_g)]/\tau_0$, $(\xi, \eta) = (x, y)/R$, $g_1 = L_{\text{Diff}}/L_{\text{Disp}}$, $g_2 = L_{\text{Diff}}/L_{\text{Nonl}}$, $g_3 = L_{\text{Diff}}\text{Re}(W_{12})E_0^2$, and $V(\xi, \eta) = [E_s(\xi, \eta)/E_0]^2$. Here U_0 , R , and E_0 are respectively the typical Rabi frequency, beam radius, and field amplitude; $L_{\text{Diff}} = \omega_p R^2/c$, $L_{\text{Disp}} = -\tau_0^2/\text{Re}(\partial^2 K/\partial \omega^2)$, and $L_{\text{Nonl}} = 1/[\text{Re}(W_{11})U_0^2]$ are respectively typical diffraction length, dispersion length, and nonlinear length.

Note that the envelope equation (4) includes dispersion, diffraction, nonlinearity, and “external” potential. When obtaining Eq. (4) we have neglected the imaginary parts of $\partial^j K/\partial \omega^j$ ($j = 1, 2$), W_{11} , and W_{12} . This is reasonable because the system works under the EIT condition $|\Omega_c|^2 \gg \gamma_{21}\gamma_{31}$ so that their imaginary parts are much smaller than their real parts. In addition, the diffraction, dispersion, and nonlinearity are assumed to be balanced, i.e., $L_{\text{Diff}} = L_{\text{Disp}} = L_{\text{Nonl}}$,

which can be achieved by taking $\tau_0 = \sqrt{-\text{Re}(\partial^2 K/\partial \omega^2)\omega_p/cR}$ and

$U_0 = \sqrt{c/[\omega_p R^2 \text{Re}(W_{11})]}$ and hence we have $g_1 = g_2 = 1$ in Eq. (4).

By taking $E_0 = 1/\sqrt{L_{\text{Diff}}\text{Re}(W_{12})}$ we also have $g_3 = 1$. The “external” potential $V(\xi, \eta)$ in Eq. (4) comes from the Stark field, which can be adjusted and hence useful to control the stability of the light bullets and vortices.

By choosing the realistic system parameters $\Omega_c = 9.0 \times 10^7 \text{ Hz}$, $\Delta_2 = -6.0 \times 10^6 \text{ Hz}$, $\Delta_3 = -2.0 \times 10^8 \text{ Hz}$, $R = 40 \text{ }\mu\text{m}$, $\tau_0 = 2.0 \times 10^{-7} \text{ s}$, $U_0 = 2.87 \times 10^7 \text{ Hz}$, and $E_0 = 3.04 \times 10^4 \text{ V/cm}$, we have $L_{\text{Diff}} \approx L_{\text{Disp}} \approx L_{\text{Nonl}} = 1.26 \text{ cm}$, and

$$\text{Re}(V_g) \approx 6.5 \times 10^{-5} c. \quad (5)$$

We see that the probe pulse propagates with an ultraslow group velocity.

Solutions of (3 + 1)D weak-light bullets and vortices. In order to obtain high-dimensional nonlinear localized solutions of the system, we assume the Stark field has the form of Bessel function, i.e.,

$$E_s(\xi, \eta) = E_{s0} J_l(\sqrt{2br}) \quad (E_{s0} \text{ and } b \text{ are real constants; } l \text{ is an integer; } r = \sqrt{\xi^2 + \eta^2}).$$
 Then Eq. (4) becomes

$$i \frac{\partial u}{\partial s} + \frac{1}{2} \left(\frac{\partial^2}{\partial \tau^2} + \frac{\partial^2}{\partial \xi^2} + \frac{\partial^2}{\partial \eta^2} \right) u + |u|^2 u + v_0 \left[J_l(\sqrt{2br}) \right]^2 u = 0, \quad (6)$$

with $v_0 = E_{s0}/E_0$. Note that Eq. (6) is similar to that obtained in Ref. 16. However, the physics here is different from that in Ref. 16 because Eq. (6) describes the nonlinear evolution of the probe-field envelope in the EIT system whereas the equation in Ref. 16 governs the dynamics of a Bose-Einstein condensate. Using the transformation

$$u = \psi \exp(i\mu s), \quad \text{Eq. (6) is reduced into } \frac{1}{2} \left(\frac{\partial^2}{\partial \tau^2} + \frac{\partial^2}{\partial \xi^2} + \frac{\partial^2}{\partial \eta^2} \right) \psi + |\psi|^2 \psi + v_0 \left[J_l(\sqrt{2br}) \right]^2 \psi = \mu \psi, \quad \text{where } \mu \text{ is a propagation constant.}$$

Fig. 2 shows the power of the probe pulse defined by $P = 2\pi \int \int \int_{-\infty}^{+\infty} |\psi|^2 d\xi d\eta d\tau$, which is a function of the propagation

constant μ and the potential strength constant v_0 . Based on the modified squared-operator method¹⁷, (3 + 1)D light bullet solutions are found numerically. Presented in Fig. 2(a) is the result of several light bullet solutions for the potential parameters $l = 0$ (i.e., the zeroth-order Bessel function) and $b = 1$. We see that for different values of v_0 ($v_0 = 1.3, 2.0, 2.7$), P always increases to a maximum firstly, and then decreases. The stability domain of the light bullet solutions is the one with $dP/d\mu > 0$ according to Vakhitov-Kokolov (VK) criterion (see ref. 17), which has been confirmed numerically by using a propagation method. The isosurfaces ($|\psi| = 0.05$) of stable light bullet solutions for ($v_0 = 1.3, \mu = 0.5$) (the red one), ($v_0 = 2.0, \mu = 1.9$) (the blue one), and ($v_0 = 2.7, \mu = 4.0$) (the green one) have been plotted in the figure.

Fig. 2(b) shows the result of a light vortex solution for the potential parameters $l = 1$ (i.e., the first-order Bessel function) and $b = 1$. The light vortex solution with quantum number of orbital angular momentum $m = 1$ is found. Because the stability domain of the vortex solution cannot be obtained by the VK criterion, a propagation method is used to study its stability. The isosurface ($|\psi| = 0.05$) and phase distribution of the vortex solution for ($v_0 = 2.7, \mu = 1.5$) are plotted in the figure. We found that the vortex solution is fairly stable during propagation in the region where $dP/d\mu > 0$.

The threshold of the optical power density \bar{P}_{max} for producing the (3 + 1)D light bullets and vortices given above can be estimated by using Poynting’s vector¹⁴. For light bullets we obtain

$$\bar{P}_{\text{max}} \approx 3.77 \times 10^{-7} W. \quad (7)$$

A similar conclusion is also obtained for light vortices. Consequently, to produce (3 + 1)D light bullets and vortices in the present system very low generation power is needed. This is drastically contrast to conventional optical media, such as glass-based optical fibers, where generation power at order of kilowatts or even larger is usually needed to produce light bullets and vortices¹⁸.

Storage and retrieval of (3 + 1)D light solitons and vortices. The principle of EIT-based LSR is well known¹⁹. When switching on the control field, probe pulse propagates in the atomic medium with nearly vanishing absorption; by slowly switching off the control

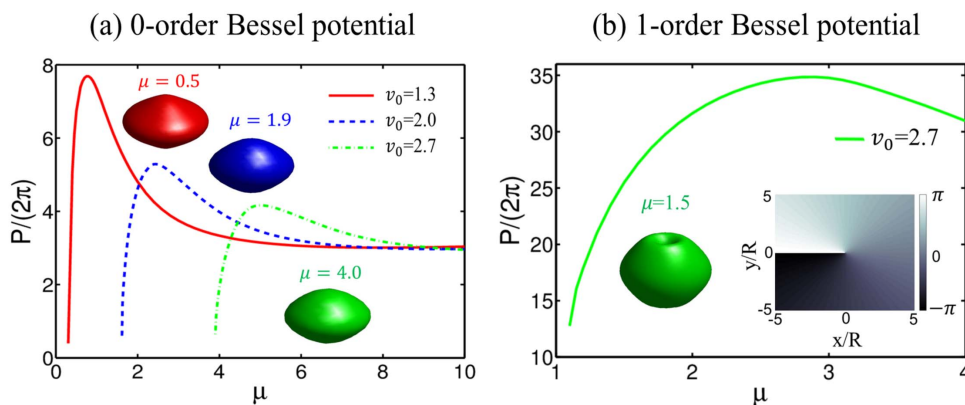


Figure 2 | Solutions of (3 + 1)D light bullets and vortices. (a) Probe-field power P of several light bullet solutions as functions of μ and v_0 , with the Stark field chosen as the zero-order Bessel function (i.e., $l = 0$). The solid, dashed, and dotted-dashed lines are for $v_0 = 1.3, 2.0$, and 2.7 , respectively. Insets give isosurface ($|\psi| = 0.05$) plots of light bullets for ($v_0 = 1.3, \mu = 0.5$; the red one), ($v_0 = 2.0, \mu = 1.9$; the blue one), and ($v_0 = 2.7, \mu = 4.0$; the green one), respectively. (b) Probe-field power P of the light vortex solution as a function of μ and v_0 , with the Stark field chosen as the first-order Bessel function (i.e., $l = 1$). The green solid line is for $v_0 = 2.7$. Insets display respectively plots of the isosurface ($|\psi| = 0.05$) for ($v_0 = 2.7, \mu = 1.5$) of the light vortex and its phase distribution in x - y plane.

field the probe pulse disappears and gets stored in the form of atomic coherence; when the control field is switched on again the probe pulse reappears. However, this principle is usually applied for linear optical pulses, which may suffer serious distortion due to the dispersion and/or diffraction. In the following we show that it is available to realize the LSR of the (3 + 1)D light bullets and vortices in our present system.

To this end, we consider the solution of the MB Eqs. (1) and (2) by using a control field that is adiabatically changed with time t to realize the function of its turning on and off. The switching-on and switching-off of the control field is modeled by the following function

$$\Omega_c = \Omega_{c0} \left\{ 1 - \frac{1}{2} \tanh \left[\frac{t - T_{\text{off}}}{T_s} \right] + \frac{1}{2} \tanh \left[\frac{t - T_{\text{on}}}{T_s} \right] \right\}, \quad (8)$$

where T_{off} and T_{on} are respectively the times of switching-off and the switching-on of the control field with a switching time T_s . The storage time of the light bullets and vortices is approximately given by $T_{\text{on}} - T_{\text{off}}$.

We first consider the LSR of the (1 + 1)D soliton pulse, corresponding the case $\partial^2/\partial\zeta^2 = \partial^2/\partial\eta^2 = 0$ and $g_3 = 0$ in Eq. (4). The result of numerical simulation on the time evolution of $|\Omega_p\tau_0|$ and atomic coherence σ_{21} as functions of z and t is presented in Fig. 3. The red solid line shown in the upper part of each panel represents the control field $|\Omega_c\tau_0|$. Here we choose $T_s/\tau_0 = 0.2$, $T_{\text{off}}/\tau_0 = 5.0$, $T_{\text{on}}/\tau_0 = 15.0$, and the other system parameters are mentioned above. The wave shape of the input probe pulse is taken as a hyperbolic secant

one, i.e., $\Omega_p(0, t) = 7.0 \text{ sech}(t/\tau_0)$. Lines 1 to 4 are for propagation distance $z = 0, 1.5, 3.0$, and 4.5 cm, respectively.

Shown in Fig. 3(a) is the result of $|\Omega_p\tau_0|$. We see that the retrieved pulse has nearly the same shape with the one before the storage. The physical reason of the shape-preservation of the probe pulse before and after the storage is due to a balance between dispersion and nonlinearity, i.e., the pulse is indeed a soliton that is rather stable during the storage and retrieval. Fig. 3(b) shows the atomic coherence σ_{21} , which has been amplified by 20 times for a better visualization. We see that σ_{21} is nonzero during the switch-off of the control field, which is a manifestation of the information transfer (i.e., storage) from the light field to the atomic ensemble.

We now turn to investigate the LSR of the (3 + 1)D light pulses. Fig. 4 shows the storage and retrieval of the light pulses with the Stark field taken to be the zero-order Bessel function (the left side of each column) and the light pulses with the Stark field taken to be the first-order Bessel function (the right side of each column) for different probe-field intensities, with the other parameters are the same as used above. Isosurfaces ($|\Omega_p\tau_0| = 0.5$) for $\Omega_{p0}\tau_0 = 2.0, 7.0, 10.0$ at $z = 0$ (before the storage), 2.25 cm (during the storage), and 4.5 cm (after the storage) are illustrated, respectively. The results are the following: (i) For the case of weak probe-field intensity (the first line in the figure), the probe pulse broadens before and after the storage; (ii) For the case of moderate probe-field intensity (the second line in the figure), the retrieved probe pulse has nearly the same shape with the one before the storage; (iii) For the case of strong probe-field

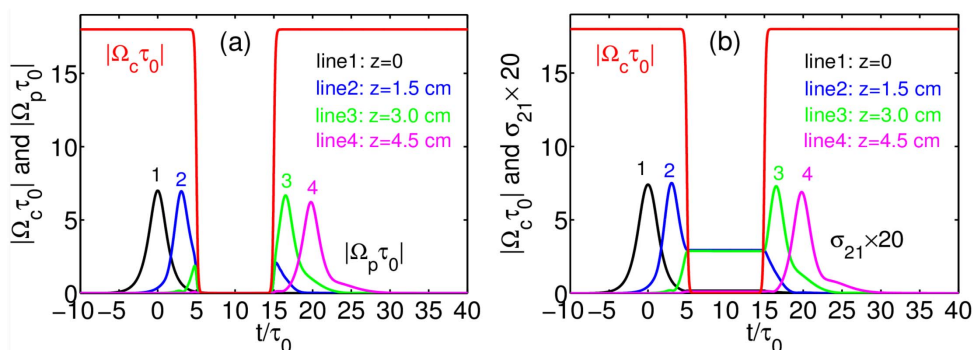


Figure 3 | Storage and retrieval of (1 + 1)D soliton pulse. (a) Evolution of $|\Omega_p\tau_0|$ and (b) atomic coherence σ_{21} as functions of z and t . For a better visualization, σ_{21} has been amplified 20 times. Lines 1 to 4 are for $z = 0, 1.5, 3.0$, and 4.5 cm, respectively. The control field $|\Omega_c\tau_0|$ is shown in the upper part of each panel.

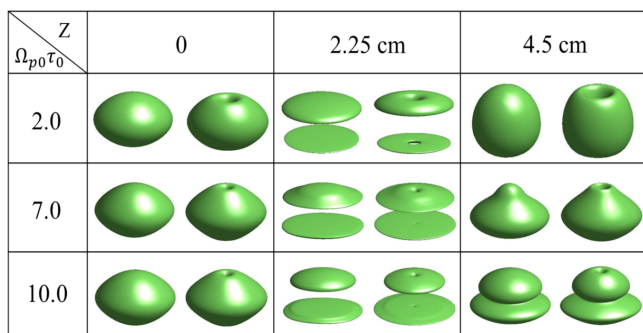


Figure 4 | Storage and retrieval of (3 + 1)D light pulses with different probe-field intensities. Storage and retrieval of (3 + 1)D light pulses with the Stark field taken to be the zero-order Bessel function (the left side of each column) and the (3 + 1)D light pulses with the Stark field taken to be the first-order Bessel function (the right side of each column) for different probe-field intensities (i.e., $\Omega_p \tau_0 = 2.0, 7.0, 10.0$) at $z = 0$ (before the storage), $z = 2.25$ cm (during the storage), and $z = 4.5$ cm (after the storage), respectively. The second line corresponds to the storage and retrieval of stable light bullets and vortices. All figures are isosurface plots with $|\Omega_p \tau_0| = 0.5$.

intensity (the third line in the figure), the retrieved probe pulse displays a serious distortion after the storage. From these results, we conclude that in the regime of the moderate probe-field intensity the storage and retrieval of (3 + 1)D light pulses are robust, which is desirable for light and quantum information processing in high dimensions. This regime is just the one where stable light bullets and vortices can form.

In order to illustrate more clearly the evolution process of the storage and retrieval of the stable (3 + 1)D light bullet and vortex (i.e., the case (ii) described above), in Fig. 5(a), Fig. 5(b), and Fig. 5(c) we show the numerical result of the evolution of the probe field ($|\Omega_p \tau_0|$) and the control field ($|\Omega_c \tau_0|$) as functions of time at $z = 0, 2.25$ cm, and 4.5 cm, respectively. We see that the light bullet and

vortex undergo steps of appearance, disappearance, and reappearance. Presented in the first (second) column of Fig. 5(d) is the light-intensity distribution in x - y plane of the bullet (vortex) for $t/\tau_0 = 5.0, 10.0,$ and $15.0,$ respectively. The third column is the phase distribution of the light vortex. The result shows that the light bullet and vortex can be stored around $t/\tau_0 = 5.0$ when the control field is switched off, and be retrieved around $t/\tau_0 = 15.0$ when the control field is switched on again. Interestingly, the phase distribution of the vortex can also be stored and retrieved, which means that the memory of the light vortex can bring more information than that of the light bullet.

We have also studied the storage and retrieval of vortices for $m = 2$. The numerical result shows that these vortices are unstable during the propagation, and hence a robust storage and retrieval of them are not available.

Discussion

From the results described above, a robust SLR for the (3 + 1)D weak-light bullets and vortices is possible by using the cold Λ -type three-level atomic system. These results can be easily generalized to other types of EIT systems with different (such as ladder-type⁸) level configurations. Furthermore, our theory can also be used to study the (3 + 1)D LSR with a Raman scheme^{20,21}, which has been suggested to obtain a broadband quantum memory of linear light pulses and has been realized recently by experiment by using the atomic ensemble working at room temperature^{22,23}.

In conclusion, we have proposed an EIT-based new scheme to realize a robust LSR for (3 + 1)D light pulses in a coherent atomic ensemble. Based on MB equations we have derived a nonlinear equation controlling the evolution of the probe-field envelope. We have shown that it is possible to obtain (3 + 1)D light bullets and vortices, which have very slow propagating velocity and ultra low generation power. We have further shown that these high-dimensional light pulses can be stabilized by using the balance between dispersion, diffraction, nonlinearity, and by a Stark laser field. We have demonstrated that these high-dimensional light pulses can be stored and retrieved very stably by switching off and on a control field. Our

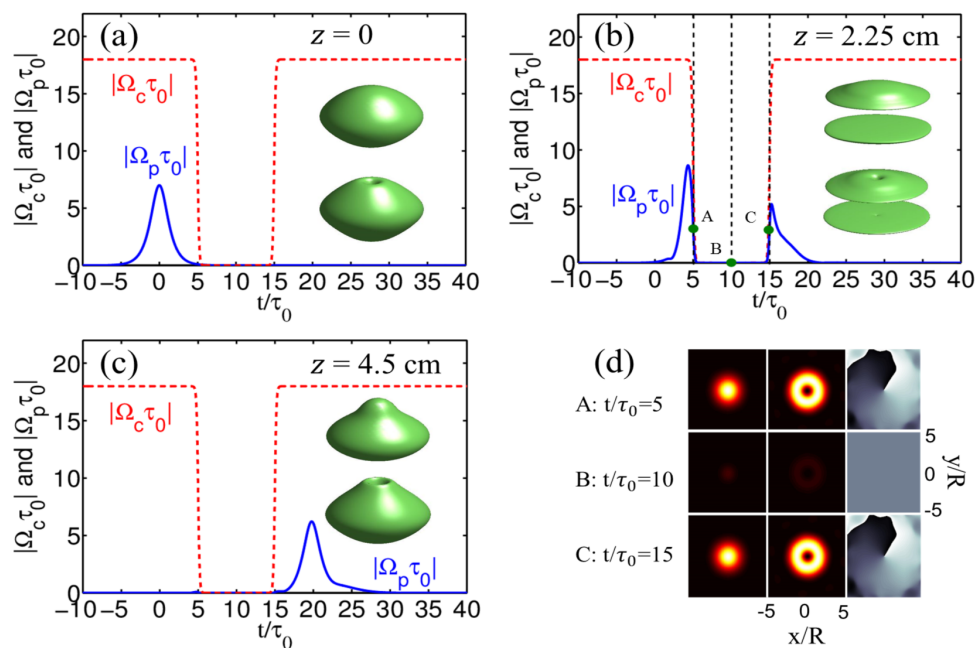


Figure 5 | Robust storage and retrieval of (3 + 1)D light bullet and vortex. (a), (b), (c) Evolutions of $|\Omega_p \tau_0|$ as function of t at the position $z = 0, z = 2.25$ cm, and $z = 4.5$ cm, respectively. Insets are isosurface plots ($|\Omega_p \tau_0| = 0.5$) of the light bullet and vortex. (d) Light-intensity distribution of the light bullet (the first column) and the vortex (the second column) in x - y plane at $t/\tau_0 = 5.0, 10.0,$ and $15.0,$ respectively. The third column shows the phase distribution of the vortex. The points A, B, C in (b) correspond to the times $t/\tau_0 = 5.0, 10.0, 15.0$ in (d).



study raise the possibility of guiding a related experiment and have potential applications in the area of light and quantum information processing.

Methods

Maxell-Bloch equations. In our semi-classical approach, MB equations are used to describe the motion of light field and atoms. Explicit expressions of the Bloch equation in the interaction picture are

$$i\frac{\partial}{\partial t}\sigma_{11} - i\Gamma_{13}\sigma_{33} + \Omega_p^*\sigma_{31} - \Omega_p\sigma_{31}^* = 0, \quad (9a)$$

$$i\frac{\partial}{\partial t}\sigma_{22} - i\Gamma_{23}\sigma_{33} + \Omega_c^*\sigma_{32} - \Omega_c\sigma_{32}^* = 0, \quad (9b)$$

$$i\frac{\partial}{\partial t}\sigma_{33} + i(\Gamma_{13} + \Gamma_{23})\sigma_{33} - \Omega_p^*\sigma_{31} + \Omega_p\sigma_{31}^* - \Omega_c^*\sigma_{32} + \Omega_c\sigma_{32}^* = 0, \quad (9c)$$

$$\left(i\frac{\partial}{\partial t} + d_{21}\right)\sigma_{21} - \Omega_p\sigma_{32}^* + \Omega_c^*\sigma_{31} = 0, \quad (9d)$$

$$\left(i\frac{\partial}{\partial t} + d_{31}\right)\sigma_{31} - \Omega_p(\sigma_{33} - \sigma_{11}) + \Omega_c\sigma_{21} = 0, \quad (9e)$$

$$\left(i\frac{\partial}{\partial t} + d_{32}\right)\sigma_{32} - \Omega_c(\sigma_{33} - \sigma_{22}) + \Omega_p\sigma_{21}^* = 0, \quad (9f)$$

where $d_{ij} = \Delta_j - \Delta_i + i\gamma_{ij}$. Dephasing rates are defined as $\gamma_{ij} = (\Gamma_j + \Gamma_i)/2 + \gamma_{ij}^{\text{col}}$ with $\Gamma_j = \sum_{E_i < E_j} \Gamma_{ij}$ being the spontaneous emission rate from the state $|j\rangle$ to all lower energy states $|i\rangle$ and γ_{ij}^{col} being the dephasing rate reflecting the loss of phase coherence between $|j\rangle$ and $|i\rangle$.

Asymptotic expansion. Assume $\sigma_{ji} = \sum_{q=0}^{\infty} \epsilon^q \sigma_{ji}^{(q)}$, with $\sigma_{ji}^{(0)} = \delta_{ji} \delta_{11}$, $\Omega_p = \sum_{q=0}^{\infty} \epsilon^q \Omega_p^{(q)}$, and $E_s = \epsilon E_s^{(1)}$. Thus $d_{ij} = d_{ij}^{(0)} + \epsilon^2 d_{ij}^{(2)}$, with $d_{ij}^{(0)} = \Delta_j - \Delta_i + i\gamma_{ij}$ and $d_{ij}^{(2)} = \frac{\alpha_j - \alpha_i}{2\hbar} |E_s^{(1)}|^2$. Here ϵ is the dimensionless small parameter characterizing the typical amplitude of the probe pulse. To obtain a divergence-free expansion, all the quantities on the right-hand side of the expansion are considered as functions of the multi-scale variables $x_1 = \epsilon x$, $y_1 = \epsilon y$, $z_q = \epsilon^q z$ ($q=0, 1, 2, \dots$), and $t_q = \epsilon^q t$ ($q=0, 1$). Substituting the expansions into Eqs. (1) and (2) and comparing the coefficients of ϵ^q , we obtain a set of linear but inhomogeneous equations which can be solved order by order.

The first order ($q=1$) solution is given by $\Omega_p^{(1)} = F e^{i\theta}$ and $\sigma_{ji}^{(1)} = \{[\delta_{j3}(\omega + \Delta_2 + i\gamma_{21}) - \delta_{j2}\Omega_c^*]/D\} F e^{i\theta}$, where $D = |\Omega_c|^2 - (\omega + \Delta_2 + i\gamma_{21})(\omega + \Delta_3 + i\gamma_{31})$ and $\theta = K(\omega)z_0 - \omega t_0$. The linear dispersion relation reads $K(\omega) = \omega/c + \kappa_{13}(\omega + \Delta_2 + i\gamma_{21})/D$. F is a yet to be determined envelope function depending on the slow variables x_1, y_1, t_1, z_1 , and z_2 .

At the second order ($q=2$), a solvability condition gives $i[\partial F/\partial z_1 + (\partial K/\partial \omega)\partial F/\partial t_1] = 0$, with $V_g = (\partial K/\partial \omega)^{-1}$. The approximation solution at this order reads

$$\sigma_{21}^{(2)} = a_{21}^{(2)} i \frac{\partial}{\partial t_1} F e^{i\theta}, \quad \sigma_{31}^{(2)} = a_{31}^{(2)} i \frac{\partial}{\partial t_1} F e^{i\theta}, \quad \sigma_{j1}^{(2)} = a_{j1}^{(2)} |F|^2 e^{-2i\alpha z_2} \quad (j=1, 2, 3), \quad \text{and}$$

$$\sigma_{32}^{(2)} = a_{32}^{(2)} |F|^2 e^{-2i\alpha z_2}, \quad \text{where}$$

$$a_{11}^{(2)} = \frac{[i\Gamma_{23} - 2|\Omega_c|^2 \left(\frac{1}{d_{32}^{(0)}} - \frac{1}{d_{32}^{(0)*}}\right)] G - i\Gamma_{13} |\Omega_c|^2 \left(\frac{1}{D d_{32}^{(0)*}} - \frac{1}{D^* d_{32}^{(0)}}\right)}{i\Gamma_{13} |\Omega_c|^2 \left(\frac{1}{d_{32}^{(0)*}} - \frac{1}{d_{32}^{(0)}}\right)}, \quad (10a)$$

$$a_{22}^{(2)} = \frac{G - i\Gamma_{13} a_{11}^{(2)}}{i\Gamma_{13}}, \quad (10b)$$

$$a_{21}^{(2)} = \frac{\Omega_c^* (2\omega + d_{21}^{(0)} + d_{31}^{(0)})}{D^2}, \quad (10c)$$

$$a_{31}^{(2)} = \frac{(\omega + d_{21}^{(0)})^2 + |\Omega_c|^2}{D^2}, \quad (10d)$$

$$a_{32}^{(2)} = \frac{\Omega_c}{d_{32}^{(0)}} \left[\frac{1}{D^*} - (a_{11}^{(2)} + 2a_{22}^{(2)}) \right], \quad (10e)$$

and $\bar{a} = \epsilon^{-2} \text{Im}[K(\omega)]$, with $G = (\omega + d_{21}^{(0)*})/D^* - (\omega + d_{21}^{(0)})/D$.

At the third order ($q=3$), a solvability condition yields the equation (3). The explicit expressions of the self- and cross-phase modulation coefficients W_{11} and W_{12} are given by

$$W_{11} = \kappa_{13} \frac{\Omega_c a_{32}^{(2)*} + (\omega + d_{21}^{(0)}) (2a_{11}^{(2)} + a_{22}^{(2)})}{D}, \quad (11a)$$

$$W_{12} = \kappa_{13} \frac{(\omega + d_{21}^{(0)})^2 (\alpha_3 - \alpha_1) + |\Omega_c|^2 (\alpha_2 - \alpha_1)}{2\hbar D^2}. \quad (11b)$$

- Simon, C. *et al.* Quantum memories. *Euro. Phys. J. D* **58**, 1–22 (2010).
- Lvovsky, A. I., Sanders, B. C. & Tittel, W. Optical quantum memory. *Nature Photon.* **3**, 706–714 (2009).
- Sangouard, N., Simon, C., de Riedmatten, H. & Gisin, N. Quantum repeaters based on atomic ensembles and linear optics. *Rev. Mod. Phys.* **83**, 33–80 (2011).
- Fleischhauer, M., Imamoglu, A. & Marangos, J. P. Electromagnetically induced transparency: Optics in coherent media. *Rev. Mod. Phys.* **77**, 633–673 (2005).
- Novikova, I., Walsworth, R. L. & Xiao, Y. Electromagnetically induced transparency-based slow and stored light in warm atoms. *Laser Photon. Rev.* **6**, 333–353 (2012).
- Bussi eres, F. *et al.* Prospective applications of optical quantum memories. *J. Mod. Opt.* **60**, 1519–1530 (2013).
- Bai, Z. Y., Hang, C. & Huang, G. Storage and retrieval of ultraslow optical solitons in coherent atomic system. *Chin. Opt. Lett.* **11**, 012701 (2013).
- Chen, Y., Bai, Z. Y. & Huang, G. Ultraslow optical solitons and their storage and retrieval in an ultracold ladder-type atomic system. *Phys. Rev. A* **89**, 023835 (2014).
- Kivshar, Y. S. & Agrawal, G. P. *Optical Solitons: From Fibers to Photonic Crystals* (Academic Press Inc., San Diego, 2003).
- Malomed, B. A., Mihalache, D., Wise, F. & Torner, L. Spatiotemporal optical solitons. *J. Opt. B: Quantum Semiclass. Opt.* **7**, R53–R72 (2005).
- Li, H., Wu, Y. & Huang, G. Stable weak light ultraslow spatio-temporal solitons via atomic coherence. *Phys. Rev. A* **84**, 033816 (2011).
- Hang, C. & Huang, G. Stern-Gerlach effect of weak-light ultraslow vector solitons. *Phys. Rev. A* **86**, 043809 (2012).
- Chen, Z. M. & Huang, G. Stern-Gerlach effect of multi-component ultraslow optical solitons via electromagnetically induced transparency. *J. Opt. Soc. Am. B* **30**, 2248–2256 (2013).
- Huang, G., Deng, L. & Payne, M. G. Dynamics of ultraslow optical solitons in a cold three-state atomic system. *Phys. Rev. E* **72**, 016617 (2005).
- Steck, D. A. Rubidium 87 D Line Data, available online at <http://steck.us/alkalidata/> (2010) Date of access: 20/05/2014.
- Mihalache, D. *et al.* Stable spatiotemporal solitons in Bessel optical lattices. *Phys. Rev. Lett.* **95**, 023902 (2005).
- Yang, J. *Nonlinear Waves in Integrable and Nonintegrable Systems* (SIAM, Philadelphia, 2010).
- Liu, X., Qian, L. J. & Wise, F. W. Generation of optical spatiotemporal solitons. *Phys. Rev. Lett.* **82**, 4631–4634 (1999).
- Fleischhauer, M. & Lukin, M. D. Dark-state polaritons in electromagnetically induced transparency. *Phys. Rev. Lett.* **84**, 5094–5097 (2000).
- Gorshkov, A. V., Andr e, A., Fleischhauer, M., Sorensen, A. S. & Lukin, M. D. Universal approach to optimal photon storage in atomic media. *Phys. Rev. Lett.* **98**, 123601 (2007).
- Nunn, J. *et al.* Mapping broadband single-photon wave packets into an atomic memory. *Phys. Rev. A* **75**, 011401(R) (2007).
- Reim, K. F. *et al.* Towards high-speed optical quantum memories. *Nature Photon.* **4**, 218–221 (2010).
- Sprague, M. R. *et al.* Broadband single-photon-level memory in a hollow-core photonic crystal fibre. *Nature Photon.* **8**, 287–291 (2014).

Acknowledgments

This work was supported by the National Natural Science Foundation of China under Grants No. 11174080, 11105052, 11204274, 11474099, and 11475063.

Author contributions

Z.C. carried out the analytical and numerical calculations. Z.B., H.-j.L. and C.H. developed primary calculating code and helped the numerical calculation. Z.C. and C.H. wrote the manuscript. G.H. conceived the idea, conducted the calculation and revised the manuscript.

Additional information

Competing financial interests: The authors declare no competing financial interests.

How to cite this article: Chen, Z., Bai, Z., Li, H.-j., Hang, C. & Huang, G. Storage and retrieval of (3 + 1)-dimensional weak-light bullets and vortices in a coherent atomic gas. *Sci. Rep.* **5**, 8211; DOI:10.1038/srep08211 (2015).



This work is licensed under a Creative Commons Attribution-NonCommercial-NoDerivs 4.0 International License. The images or other third party material in this article are included in the article's Creative Commons license, unless indicated otherwise in the credit line; if the material is not included under the Creative

Commons license, users will need to obtain permission from the license holder in order to reproduce the material. To view a copy of this license, visit <http://creativecommons.org/licenses/by-nc-nd/4.0/>